Supplementary information

Synthesis and photophysical properties of rare earth complexes bearing silanediamido ligands $SiMe_2(NAr)_2^{2-}$ (Ar = Dipp, Mes)

Olga A. Mironova*[a], Daniil I. Lashchenko[a,b], Aleksey A. Ryadun[a], Taisiya S. Sukhikh[a], Denis A. Bashirov*[a], Nikolay A. Pushkarevsky[a], Sergey N. Konchenko[a]
Nikolaev Institute of Inorganic Chemistry SB RAS, Akademika Lavrentieva Ave. 3, 630090 Novosibirsk, Russia.
Department of Natural Sciences, Novosibirsk State University, Pirogova St. 2, 630090 Novosibirsk, Russia.
Corresponding authors at: Nikolaev Institute of Inorganic Chemistry SB RAS, Akademika Lavrentieva Ave. 3, 630090 Novosibirsk, Russia. E-mail: mironova@niic.nsc.ru (O.A. Mironova), bashirov@niic.nsc.ru (D.A. Bashirov)

Table of contents:

1. X-ray structural determination

Table S1 Crystal data and structure refinement for the compounds.

Identification code	**Y^{Dipp}**	**Tb^{Dipp}**	**Gd^{Dipp}**	**Y^{Mes}**	**Gd^{Mes}**	**Tb^{Mes}**	**2Y^{Dipp}**	**3Y^{Dipp}**
Empirical formula	$C_{68}H_{112}Cl_2N_4O_4Si_2Y_2$	$C_{68}H_{112}Cl_2N_4O_4Si_2Tb_2$	$C_{68}H_{112}Cl_2N_4O_4Si_2Sm_2$	$C_{56}H_{88}Cl_2N_4O_4Si_2Y_2$	$C_{56}H_{88}Cl_2Gd_2N_4O_4Si_2$	$C_{56}H_{88}Cl_2N_4O_4Si_2Tb_2$	$C_{88}H_{152}Cl_4Li_2N_4O_9Si_2Y_2$	$C_{38}H_{64}ClN_2O_3SiY$
Formula weight	1354.51	1494.53	1477.39	1186.20	1322.88	1326.22	1799.81	749.36
Temperature/K	150(2)	150(2)	150(2)	150(2)	150(2)	150(2)	150(2)	150(2)
Crystal system	orthorhombic	orthorhombic	orthorhombic	orthorhombic	orthorhombic	orthorhombic	monoclinic	triclinic
Space group	*Pbca*	*Pbca*	*Pbca*	*Pbca*	*Pbca*	*Pbca*	$P2_1/n$	$P\bar{1}$
a/Å	18.5551(16)	18.5890(3)	18.671(3)	17.2844(15)	17.3771(18)	17.3121(4)	12.6828(18)	10.178(3)
b/Å	17.539(2)	17.5439(4)	17.547(2)	15.8628(15)	15.9355(13)	15.9196(4)	18.077(2)	12.127(3)
c/Å	21.8449(17)	21.9363(4)	21.967(3)	21.879(2)	21.937(2)	21.8917(5)	21.843(3)	16.974(4)
α/°	90	90	90	90	90	90	90	97.009(8)
β/°	90	90	90	90	90	90	95.133(5)	96.301(7)
γ/°	90	90	90	90	90	90	90	106.915(7)
Volume/Å^3	7109.0(13)	7153.9(2)	7197.0(17)	5998.9(10)	6074.6(10)	6033.4(2)	4987.7(12)	1966.2(9)
Z	4	4	4	4	4	4	2	2
ρ_{calc}g/cm^3	1.266	1.388	1.363	1.313	1.446	1.460	1.198	1.266
μ/mm^{-1}	1.780	2.116	1.769	2.099	2.337	2.498	1.340	1.618
F(000)	2880.0	3088.0	3064.0	2496.0	2696.0	2704.0	1920.0	800.0
Crystal size/mm^3	0.3 × 0.3 × 0.3	0.32 × 0.32 × 0.26	0.135 × 0.09 × 0.08	0.2 × 0.2 × 0.1	0.14 × 0.13 × 0.08	0.15 × 0.15 × 0.1	0.21 × 0.18 × 0.1	0.22 × 0.21 × 0.18
Radiation	MoKα (λ = 0.71073)	MoKα (λ = 0.71073)	MoKα (λ = 0.71073)	MoKα (λ = 0.71073)	MoKα (λ = 0.71073)	MoKα (λ = 0.71073)	MoKα (λ = 0.71073)	MoKα (λ = 0.71073)
2Θ range for data collection/°	4.328 to 50.116	4.312 to 52.748	4.302 to 51.36	3.952 to 48.808	3.934 to 59.17	5.092 to 55.772	4.37 to 48.81	2.446 to 48.81
Index ranges	$-22 \le h \le 19$, $-17 \le k \le 20$, $-21 \le l \le 26$	$-23 \le h \le 18$, $-12 \le k \le 21$, $-27 \le l \le 20$	$-22 \le h \le 22$, $-21 \le k \le 21$, $-26 \le l \le 26$	$-20 \le h \le 18$, $-18 \le k \le 18$, $-25 \le l \le 22$	$-24 \le h \le 24$, $-21 \le k \le 21$, $-30 \le l \le 30$	$-14 \le h \le 22$, $-20 \le k \le 17$, $-25 \le l \le 18$	$-14 \le h \le 14$, $-17 \le k \le 21$, $-25 \le l \le 25$	$-11 \le h \le 11$, $-14 \le k \le 12$, $-19 \le l \le 19$
Reflections collected	27569	24694	62745	41594	55725	17555	44099	15308
Independent reflections	6278 [R_{int} = 0.0574, R_{sigma} = 0.0579]	7292 [R_{int} = 0.0364, R_{sigma} = 0.0416]	6832 [R_{int} = 0.1006, R_{sigma} = 0.0526]	4931 [R_{int} = 0.1127, R_{sigma} = 0.0681]	8505 [R_{int} = 0.0578, R_{sigma} = 0.0370]	6101 [R_{int} = 0.0514, R_{sigma} = 0.0529]	8197 [R_{int} = 0.1552, R_{sigma} = 0.1291]	6425 [R_{int} = 0.0760, R_{sigma} = 0.1420]
Data/restraints/parameters	6278/21/390	7292/15/390	6832/21/390	4931/0/324	8505/0/324	6101/0/324	8197/140/504	6425/9/430
Goodness-of-fit on F^2	1.007	1.010	1.280	1.011	1.021	1.026	1.059	0.975
Final R indexes [I>=2σ (I)]	R_1 = 0.0375, wR_2 = 0.0809	R_1 = 0.0284, wR_2 = 0.0612	R_1 = 0.0619, wR_2 = 0.1504	R_1 = 0.0401, wR_2 = 0.0790	R_1 = 0.0266, wR_2 = 0.0574	R_1 = 0.0347, wR_2 = 0.0750	R_1 = 0.0743, wR_2 = 0.1676	R_1 = 0.0546, wR_2 = 0.0867
Final R indexes [all data]	R_1 = 0.0758, wR_2 = 0.0920	R_1 = 0.0501, wR_2 = 0.0693	R_1 = 0.0923, wR_2 = 0.1704	R_1 = 0.0846, wR_2 = 0.0941	R_1 = 0.0384, wR_2 = 0.0639	R_1 = 0.0539, wR_2 = 0.0847	R_1 = 0.1385, wR_2 = 0.1976	R_1 = 0.1151, wR_2 = 0.1020
Largest diff. peak/hole / e Å^{-3}	0.37/-0.37	0.92/-0.58	2.46/-1.57	0.32/-0.52	0.81/-0.41	0.61/-0.39	1.00/-0.57	0.40/-0.53

2. NMR spectroscopy

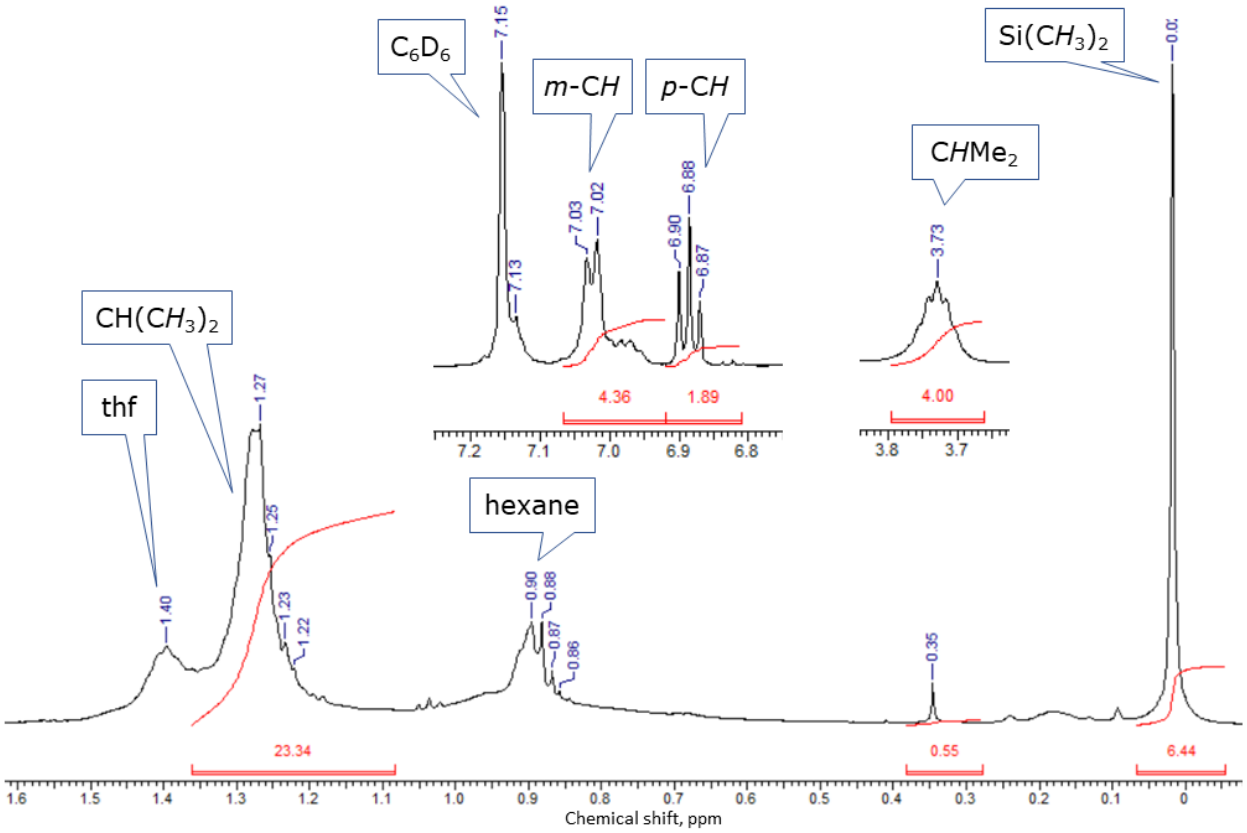

Figure S1 ^{1}H NMR spectrum of the product of the reaction of H_2L^{Dipp} with ^{n}BuLi in hexane, C_6D_6.

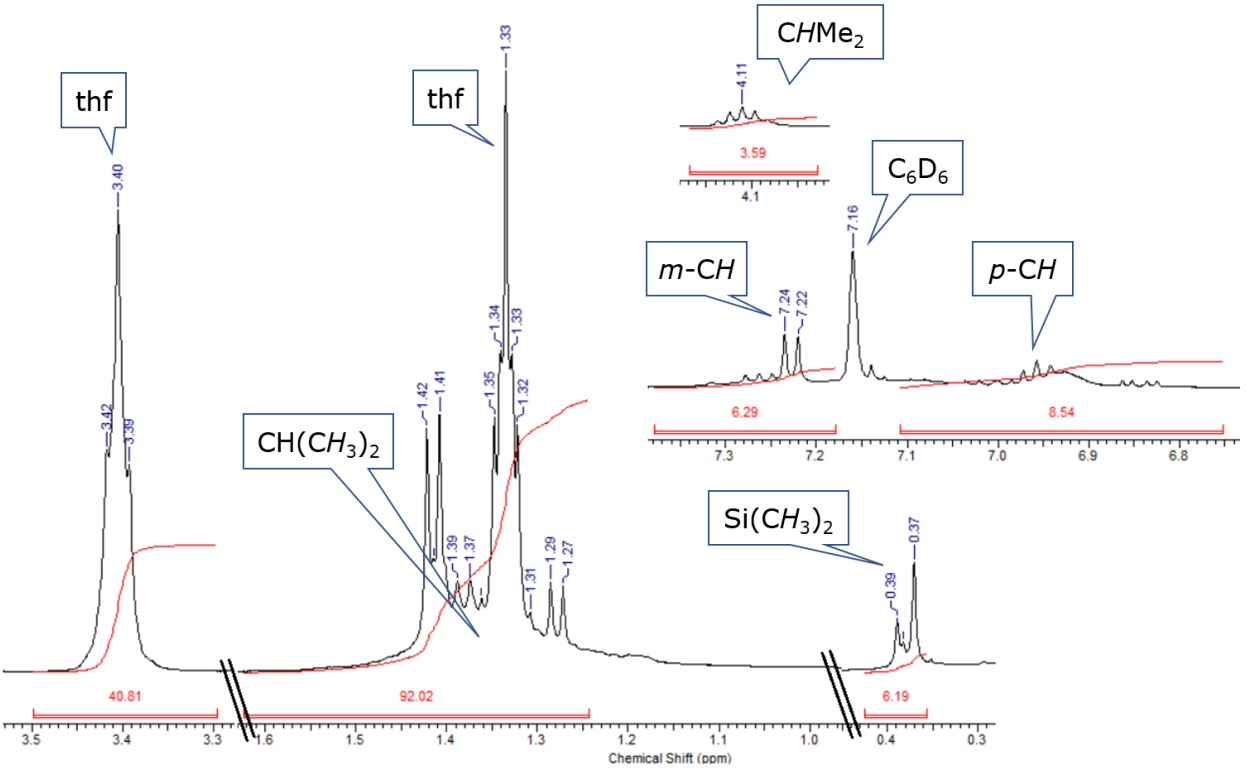

Figure S2 ^{1}H NMR spectrum of the product of the reaction of H_2L^{Dipp} with ^{n}BuLi in thf; the several signals corresponding to the same groups are conditioned by the non-equivalence of Dipp substituents due to the coordination of thf.

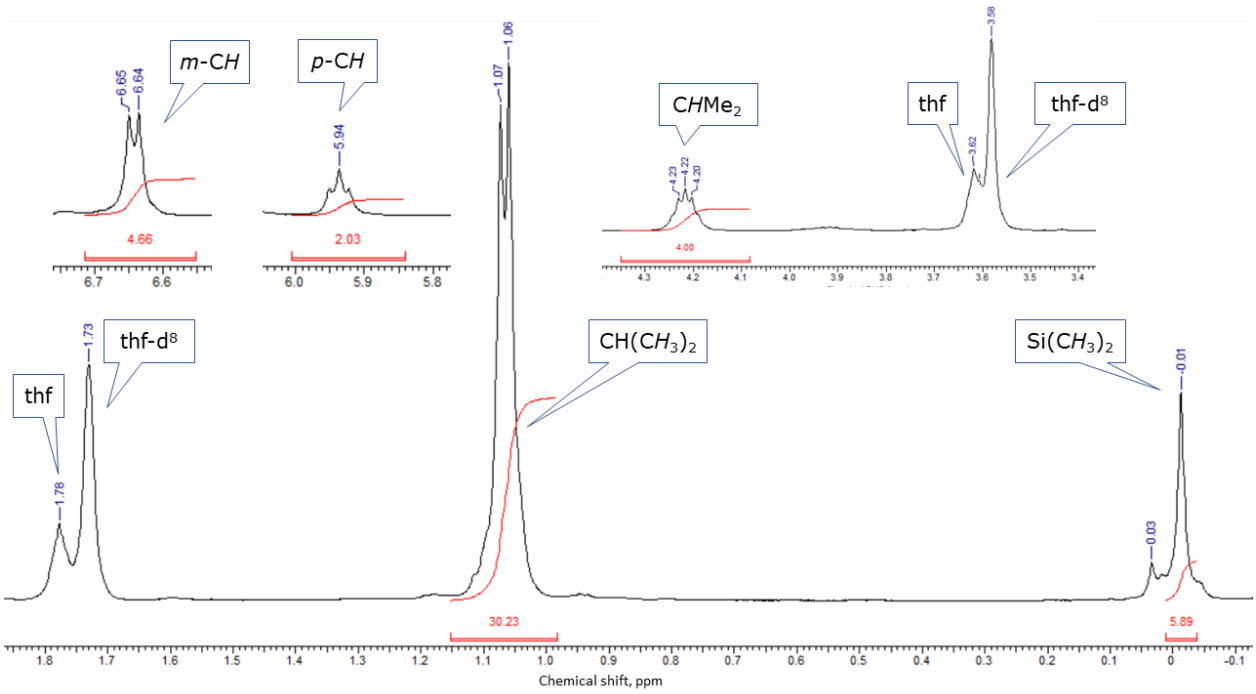

Figure S3 ^{1}H NMR spectrum of **K_2L^{Dipp}** in thf-d^{8}: the salt was obtained by the reaction of KH and proligand in THF.

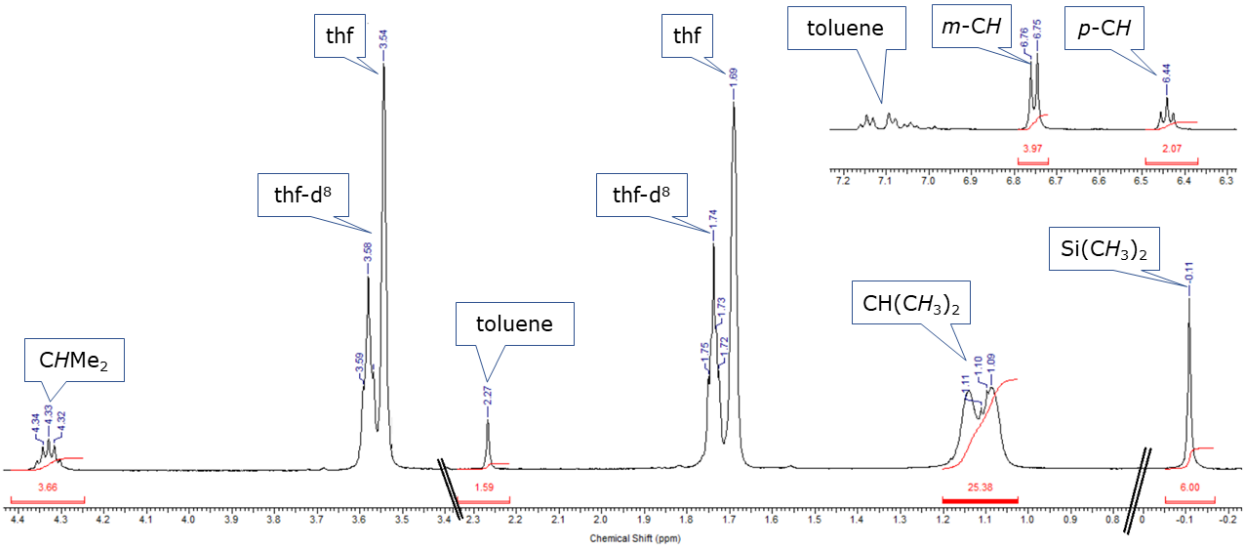

Figure S4 ^{1}H NMR spectrum of **Y^{Dipp}** in thf-d^{8}.

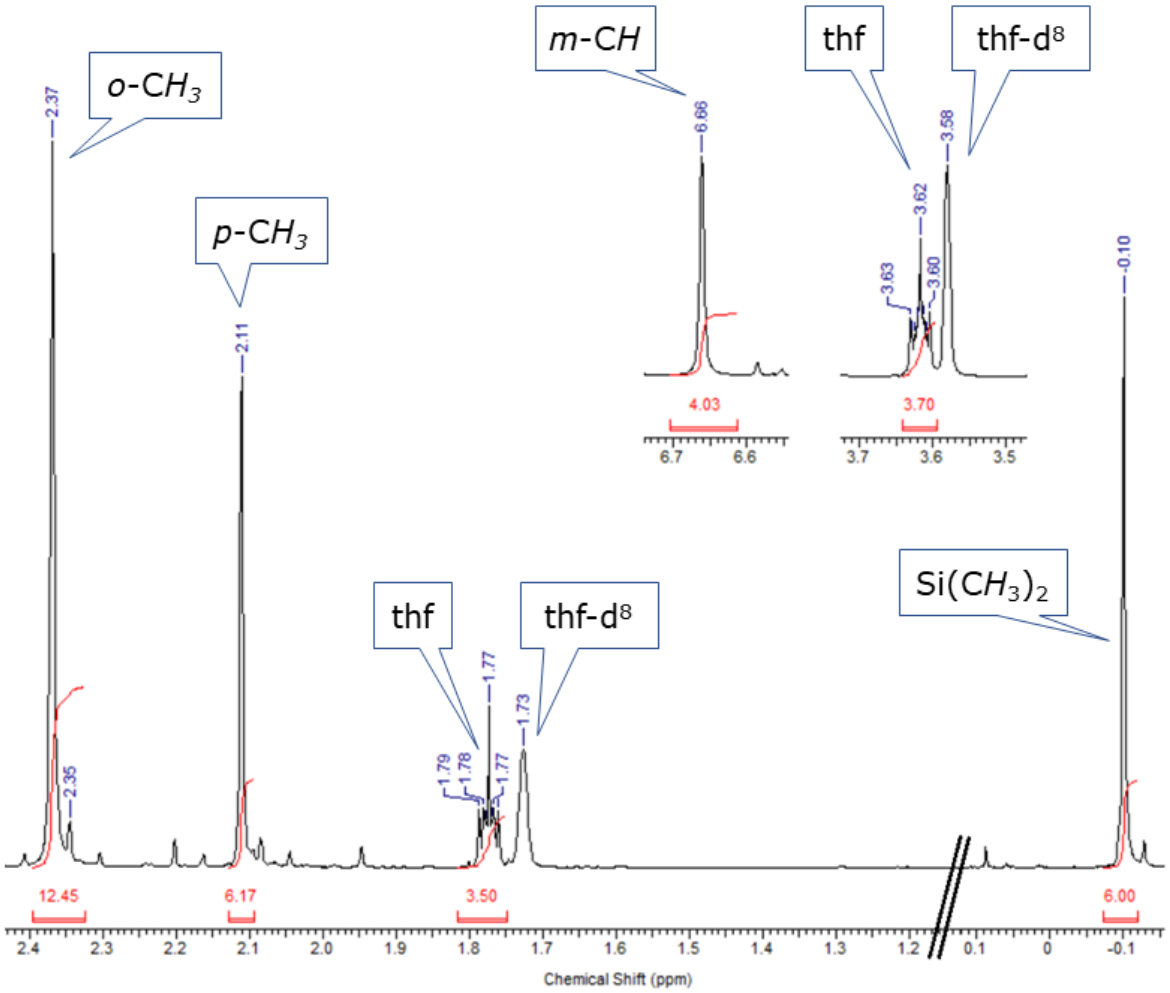

Figure S5 ^{1}H NMR spectrum of $\mathbf{Y^{Mes}}$ in thf-d^{8}.

3. Powder X-ray studies

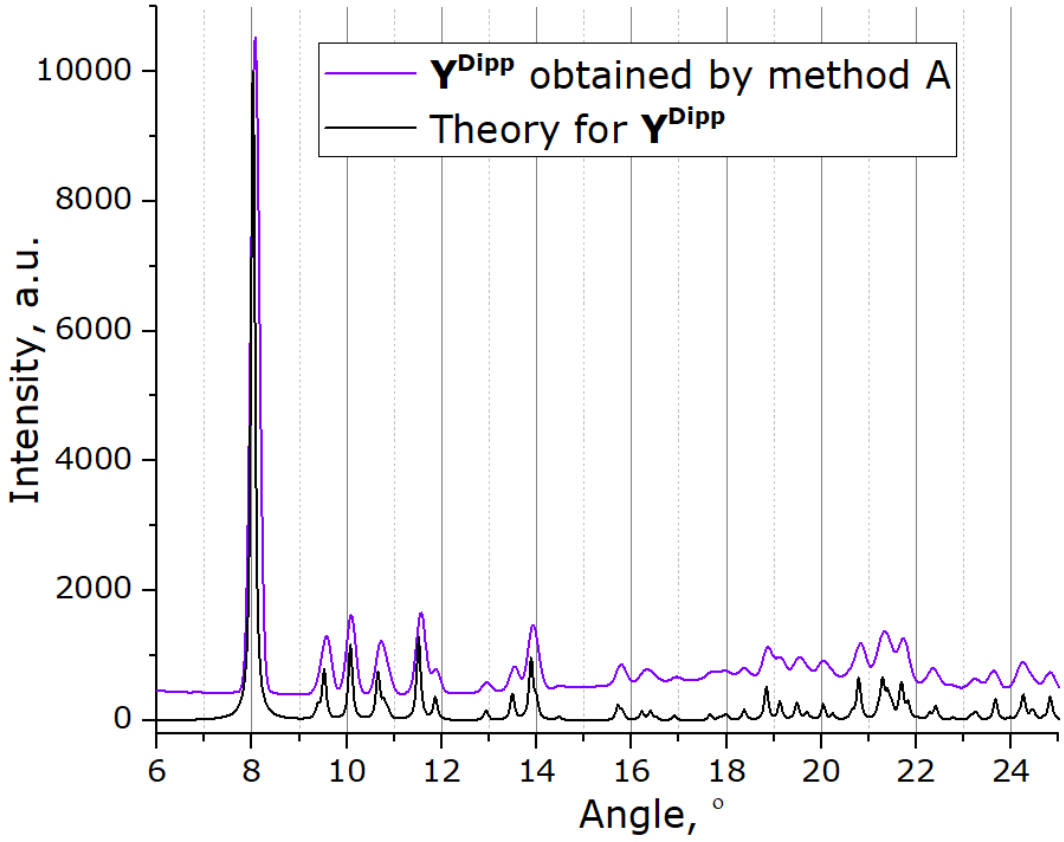

Figure S6 The experimental and simulated powder XRD patterns for $\mathbf{Y^{Dipp}}$ obtained by method A (Cu Kα radiation).

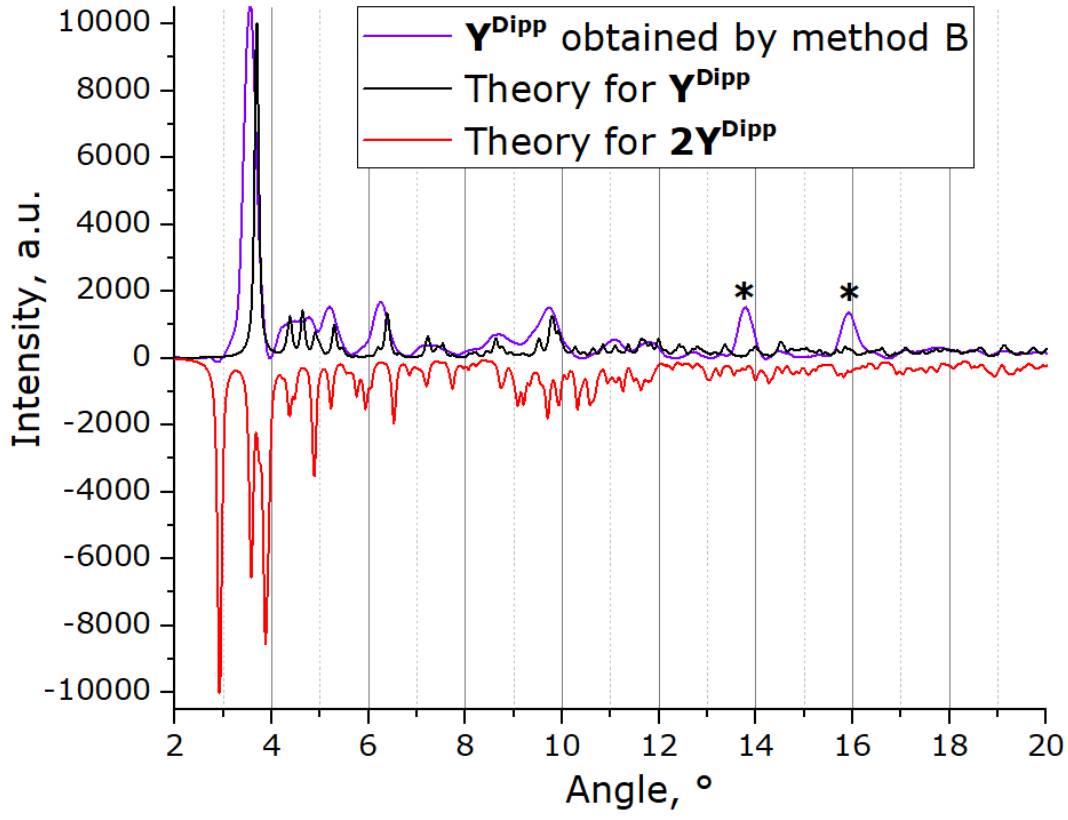

Figure S7 The experimental and simulated XRD patterns for $\mathbf{Y^{Dipp}}$ obtained by method B (Mo Kα radiation). The marked peaks are presumably attributed to LiCl.

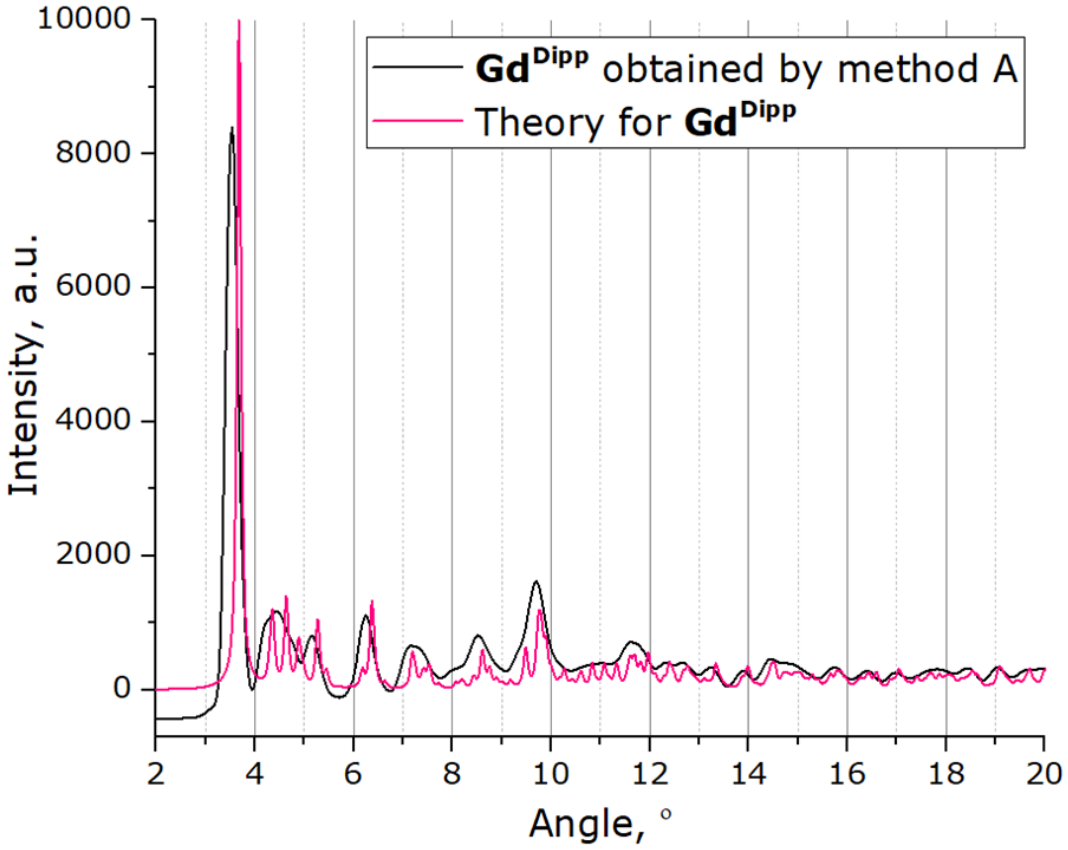

Figure S8 The experimental and simulated XRD patterns for **Gd^{Dipp}** obtained by method A (Mo Kα radiation).

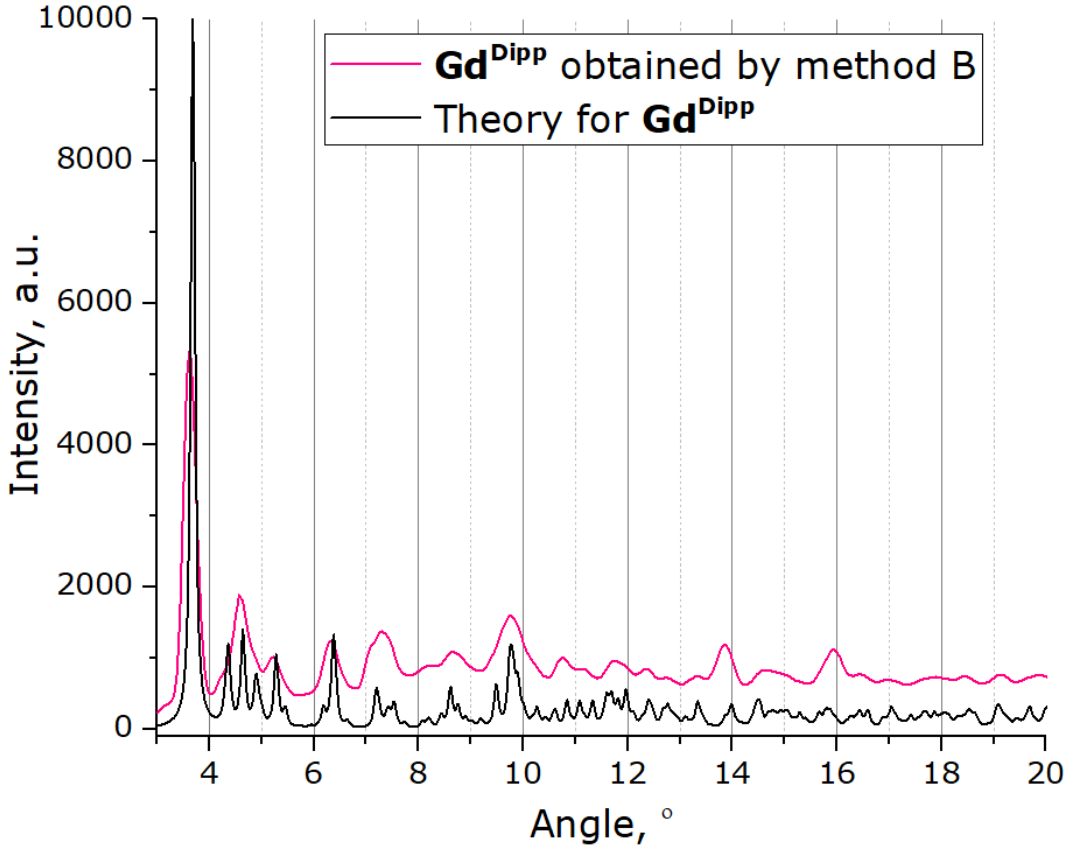

Figure S9 The experimental and simulated XRD patterns for **Gd^{Dipp}** obtained by method B (Mo Kα radiation).

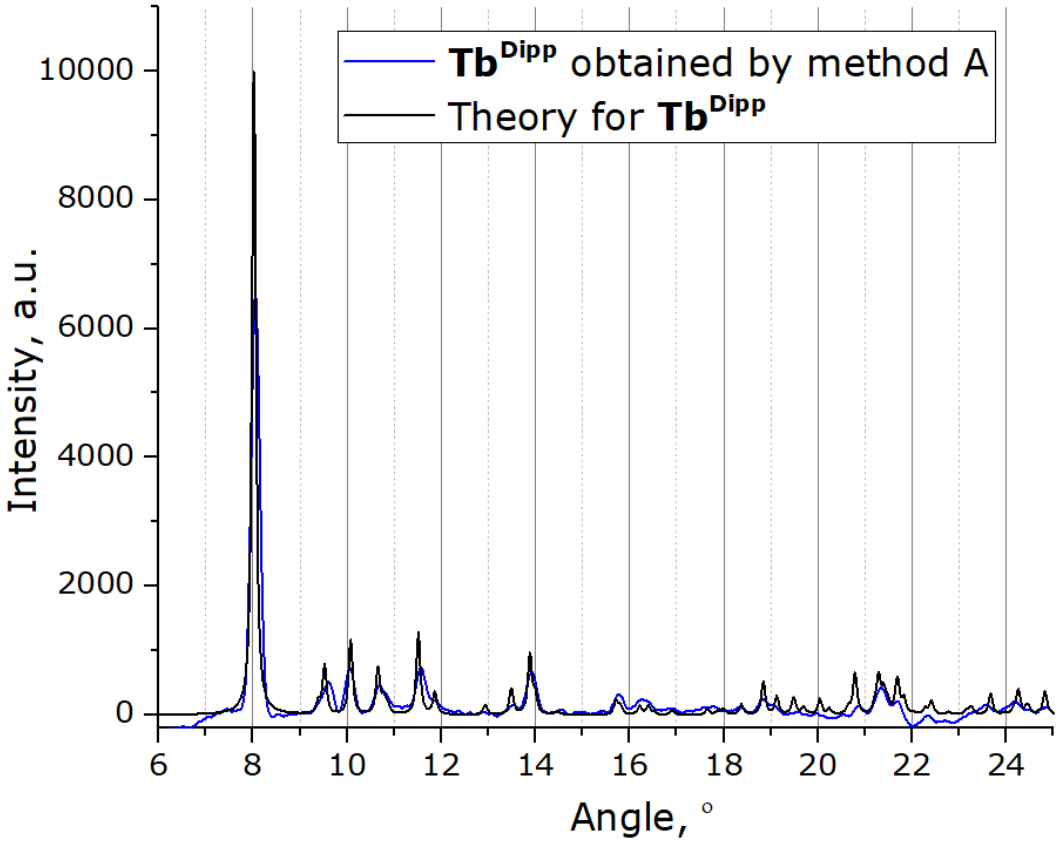

Figure S10 The experimental and simulated XRD patterns for **Tb^{Dipp}** obtained by method A (Cu Kα radiation).

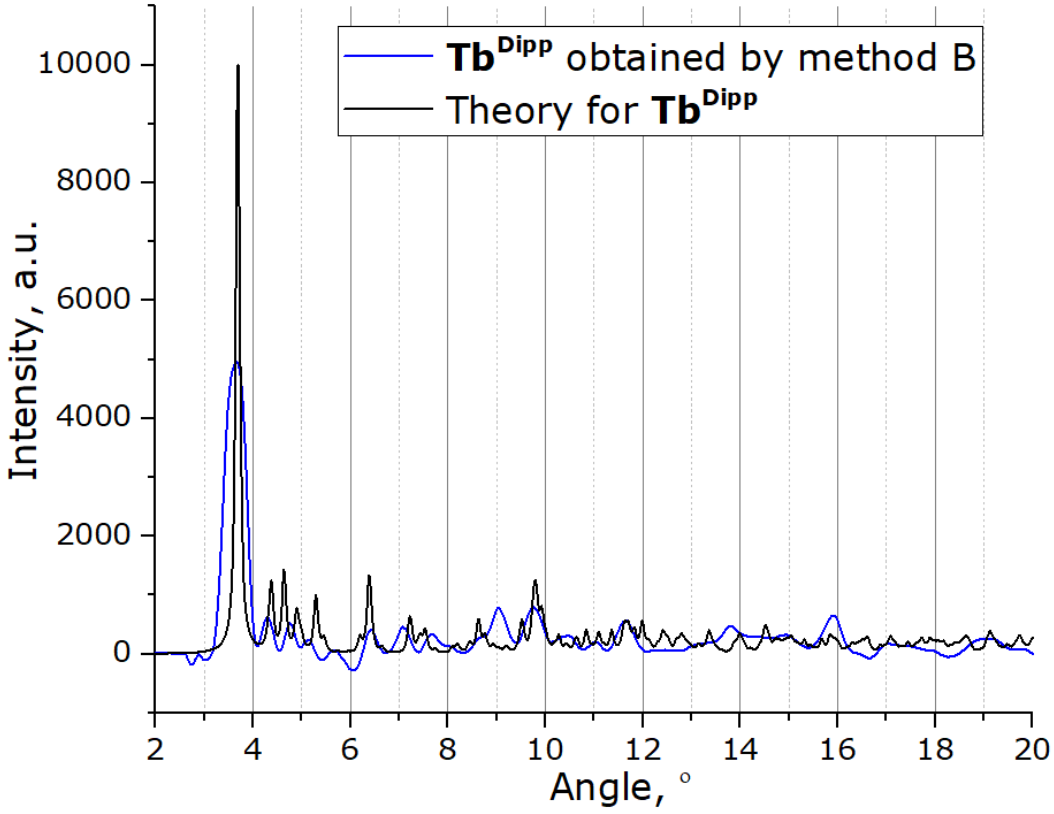

Figure S11 The experimental and simulated XRD patterns for **Tb^{Dipp}** obtained by method B (Mo Kα radiation).

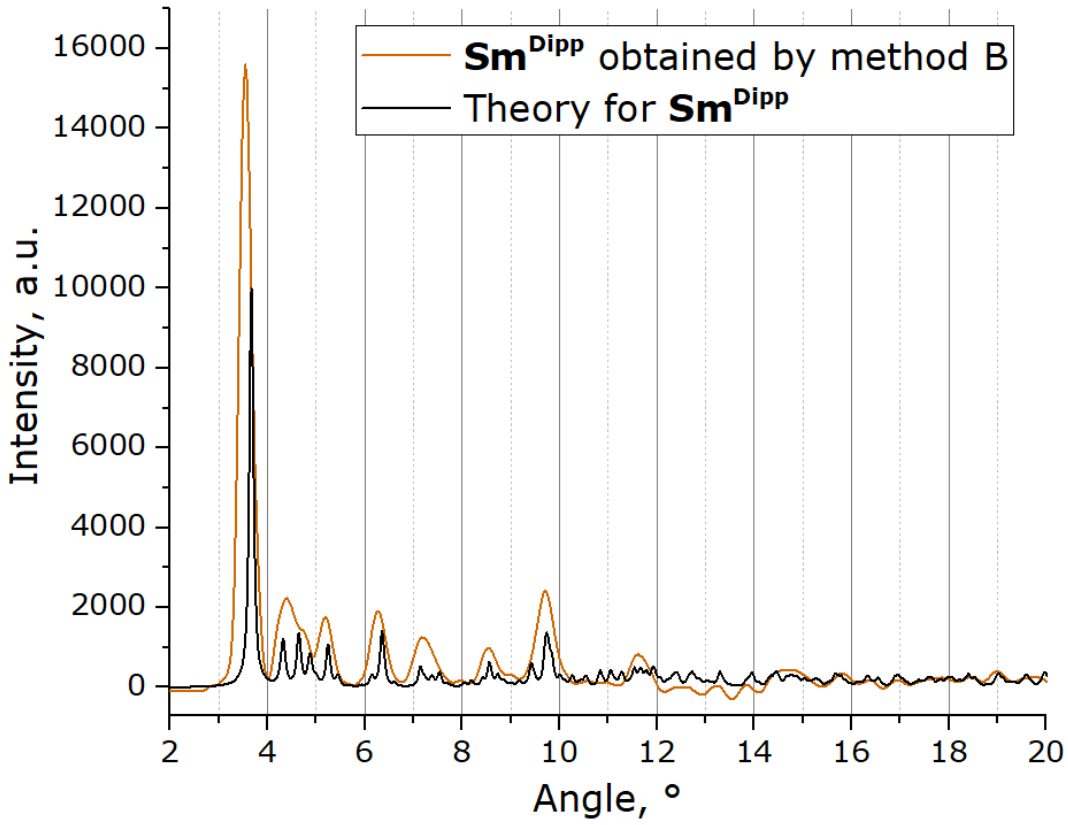

Figure S12 The experimental and simulated XRD patterns for Sm^{Dipp} obtained by method B (Mo Kα radiation).

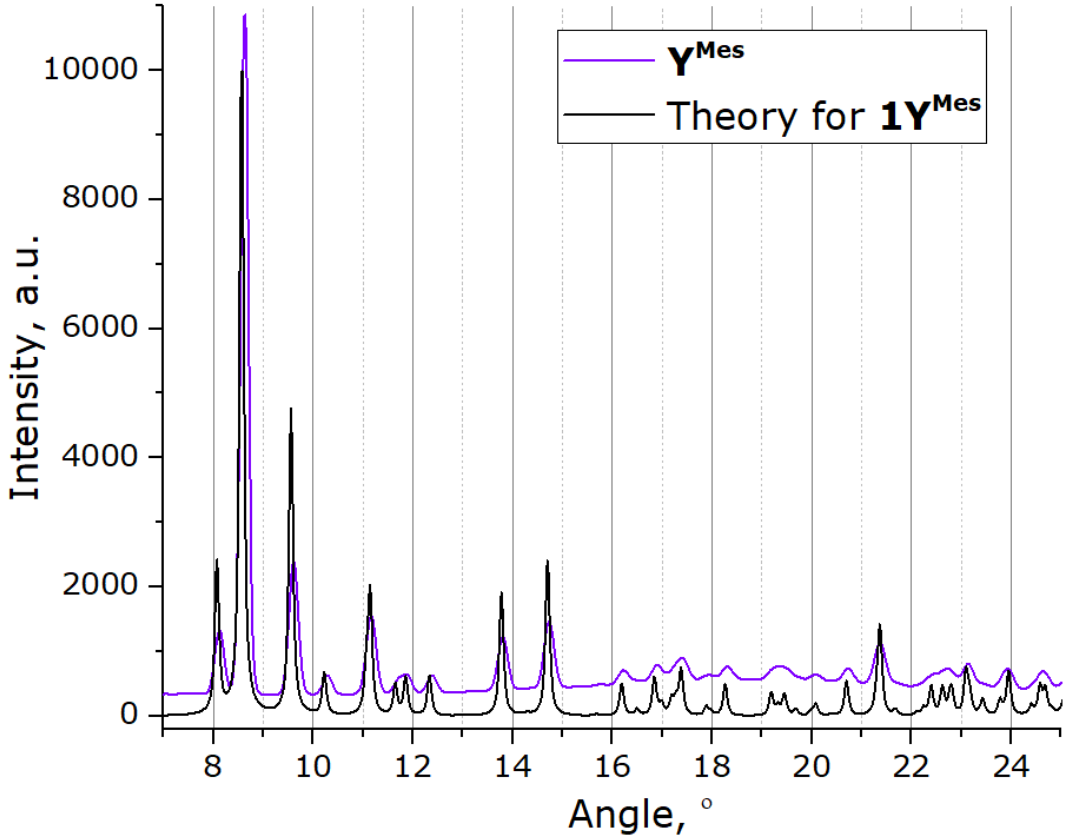

Figure **S13** The experimental and simulated XRD patterns for Y^{Mes} (Cu Kα radiation).

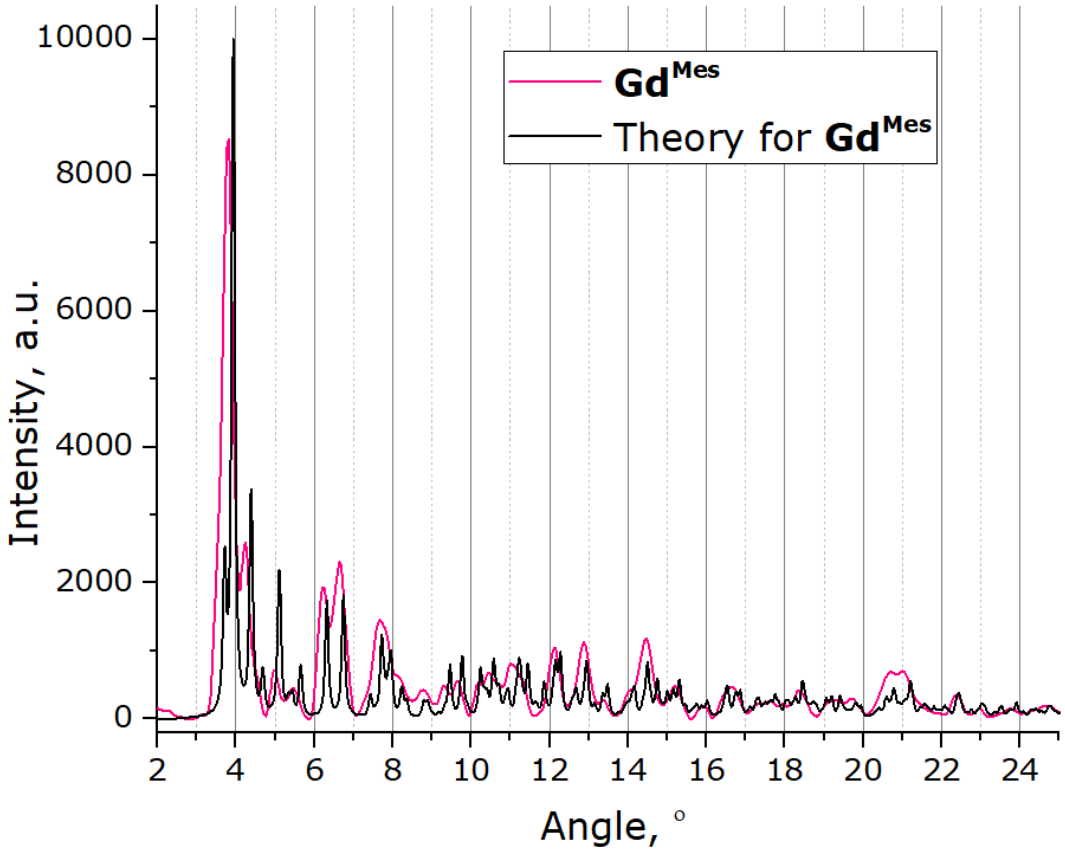

Figure S14 The experimental and simulated XRD patterns for **Gd**^{Mes} (Mo Kα radiation).

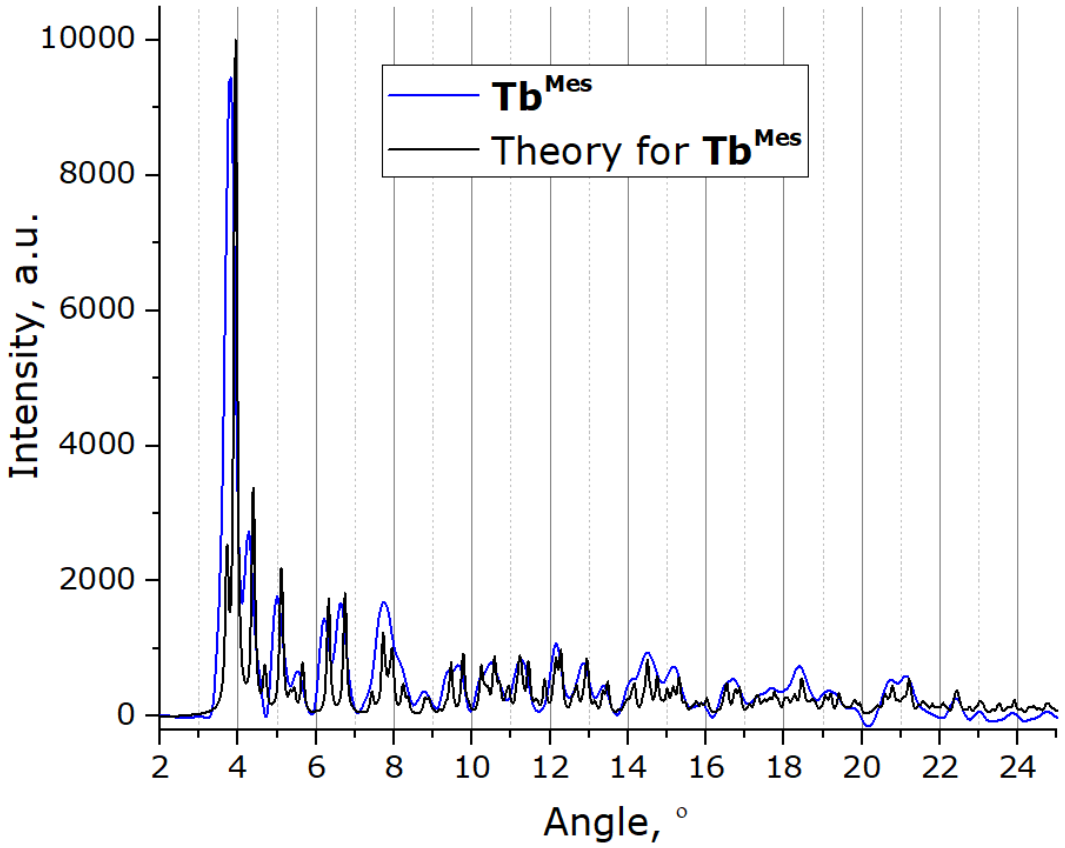

Figure S15 The experimental and simulated XRD patterns for **Tb**^{Mes} (Mo Kα radiation).

4. Electronic absorption spectra

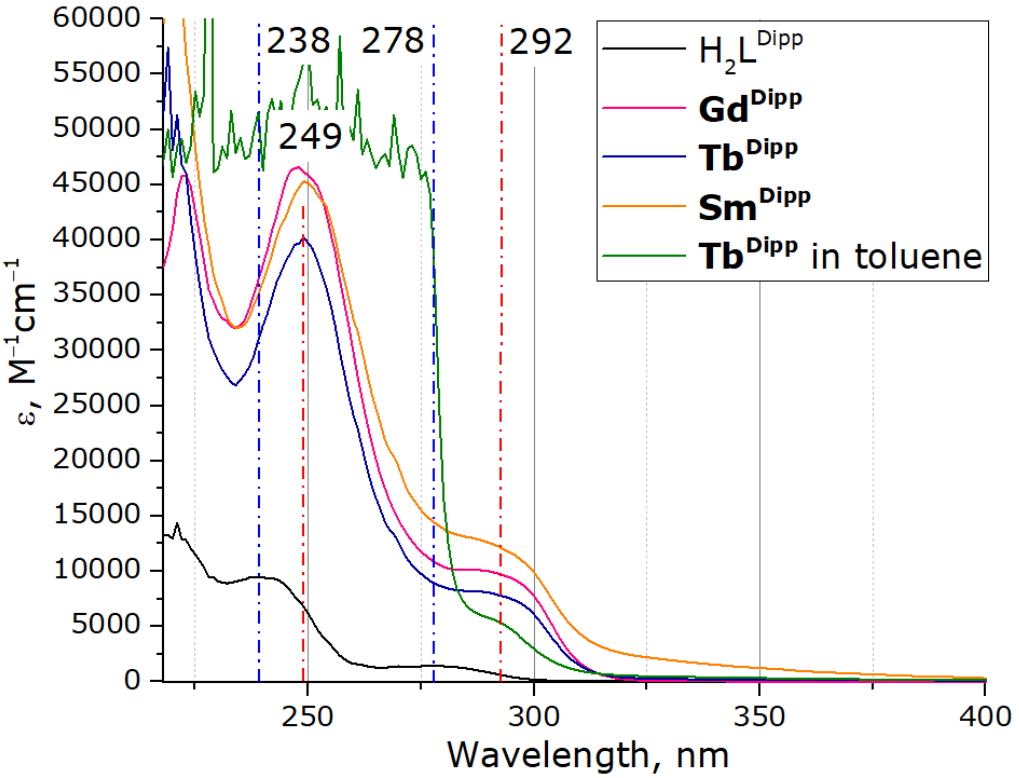

Figure S16 Electronic absorption spectra of the proligand H_2L^{Dipp} and its lanthanide complexes in thf solutions or in toluene solution in the case of $\mathbf{Tb^{Dipp}}$. For the latter, the off-scale in the UV region is conditioned by the absorption of toluene.

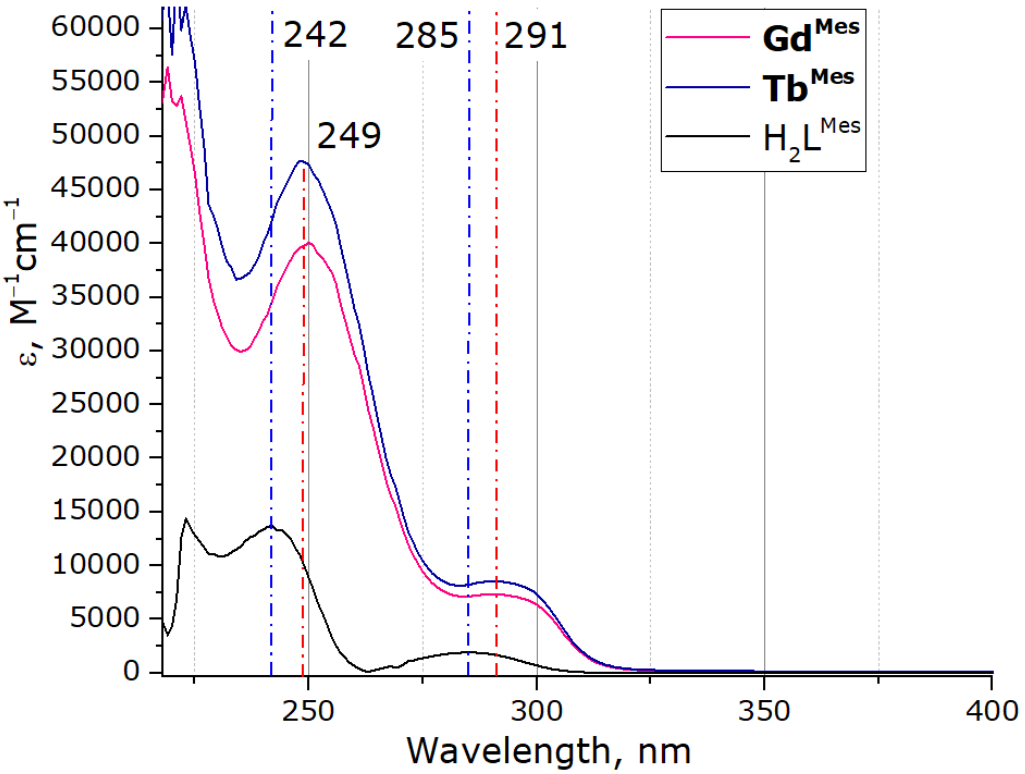

Figure S17 Electronic absorption spectra of the proligand H_2L^{Mes} and its lanthanide complexes in thf solutions.

5. Luminescence study

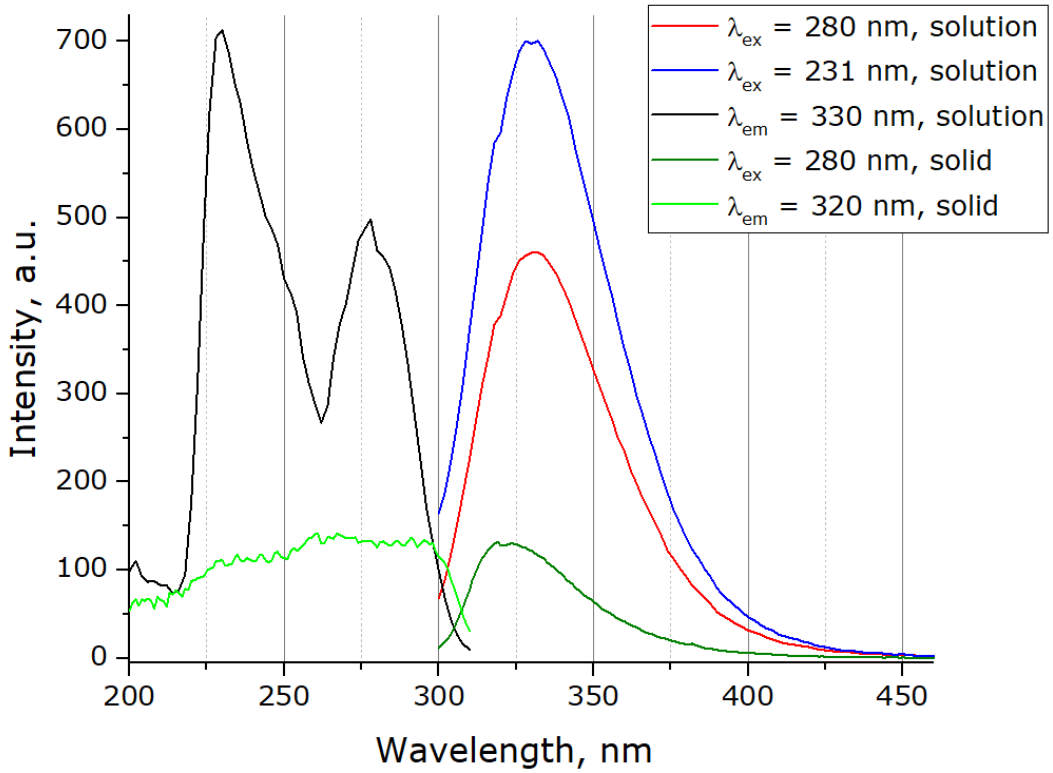

Figure S18 Excitation (left) and emission (right) spectra of H_2L^{Dipp} in the solid state and thf solution. For the solution, C = $1.3 \cdot 10^{-4}$ M, 1 cm cuvette, slit widths 5×5mm. For the solid, slit widths 1.5×2.5 nm.

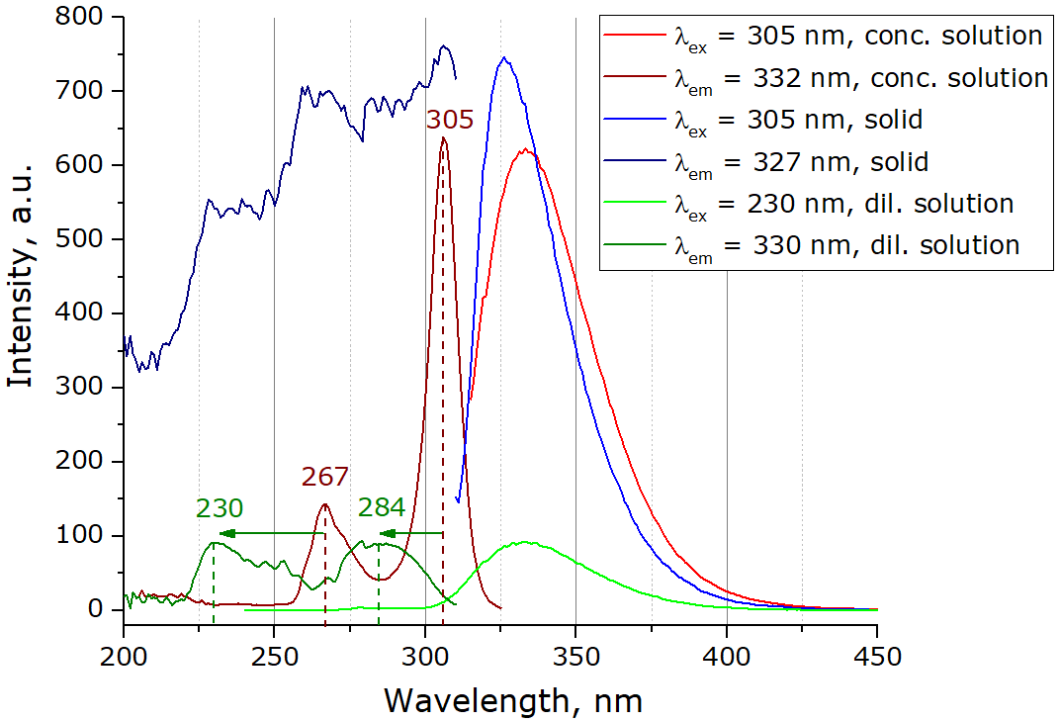

Figure S19 Excitation (left) and emission (right) spectra of H_2L^{Mes} in the solid state and thf solutions. For the concentrated solution, C = $3.1 \cdot 10^{-3}$ M; for the diluted solution, C = $1.3 \cdot 10^{-4}$ M; 1 cm cuvette. Slit widths 2.5×2.5 nm.

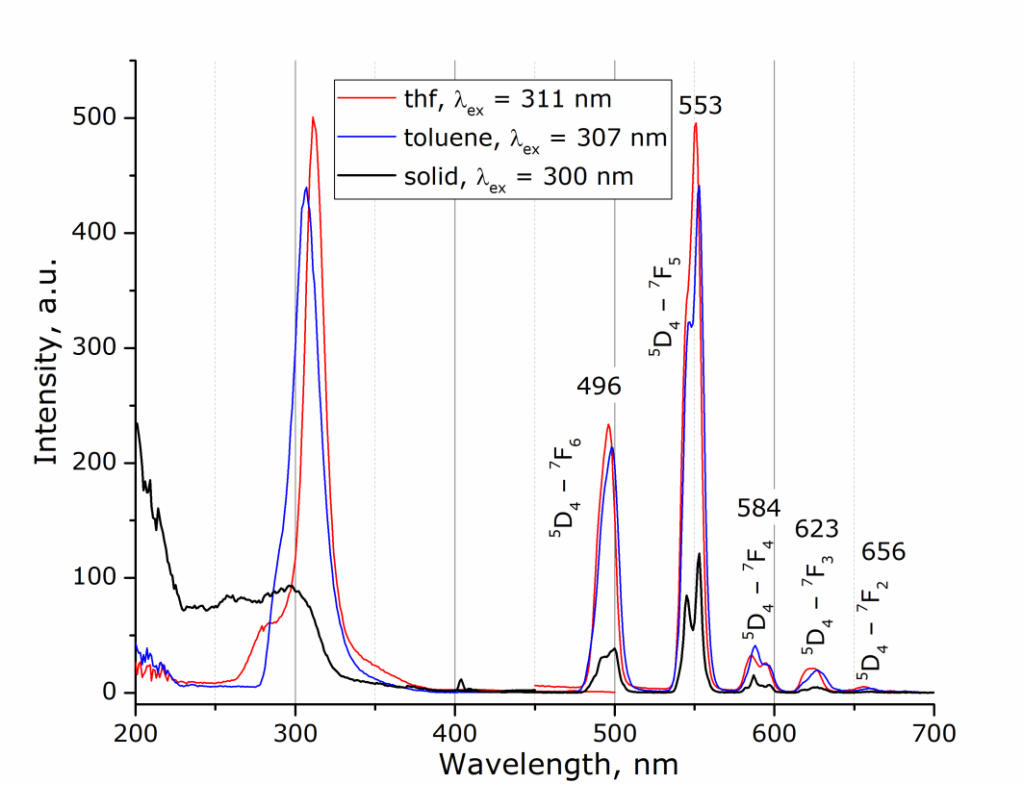

Figure S20 Excitation (left) and emission (right) spectra of **Tb^{Dipp}** in the solid state and thf and toluene solutions. For the solution, 1 cm cuvette, C(thf) = $6.9 \cdot 10^{-4}$ M, C(toluene) = $6.7 \cdot 10^{-4}$ M. Slit widths 5×5 nm for solutions, 2.5×2.5 nm for solid.

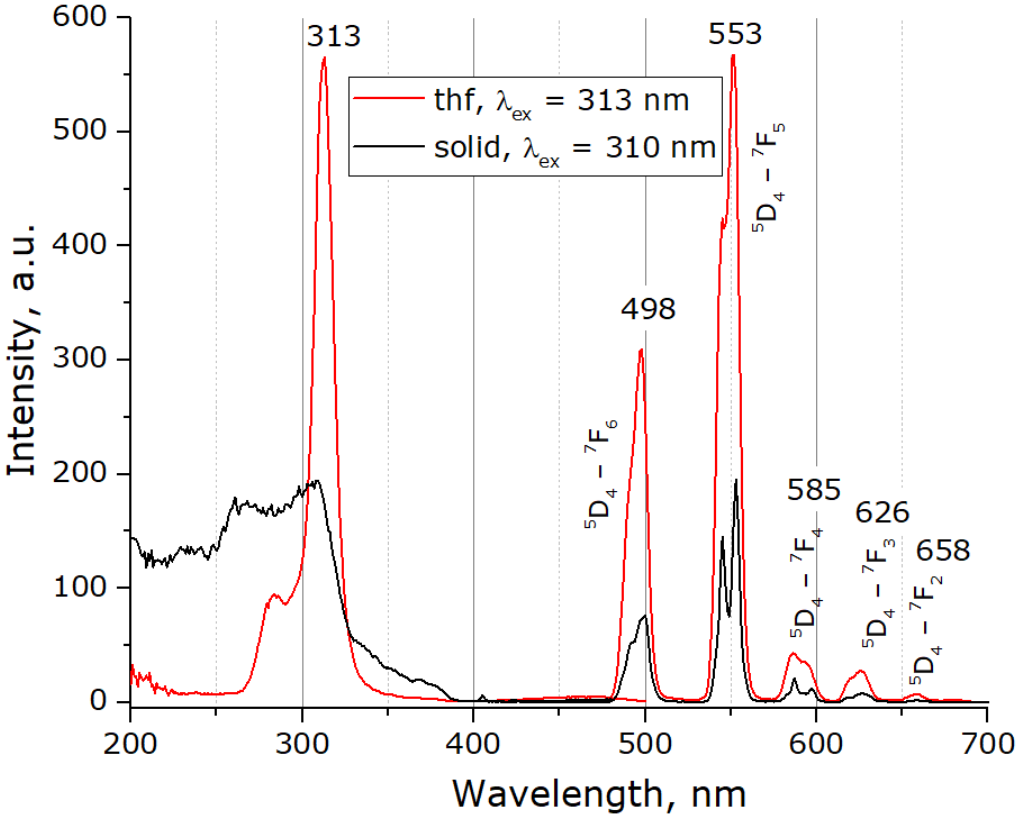

Figure S21 Excitation (left) and emission (right) spectra of **Tb^{Mes}** in the solid state and thf solution. For the solution, 1 cm cuvette, slit widths 5×5nm, C = $6.0 \cdot 10^{-4}$ M. For the solid, slit widths 2.5×2.5 nm.

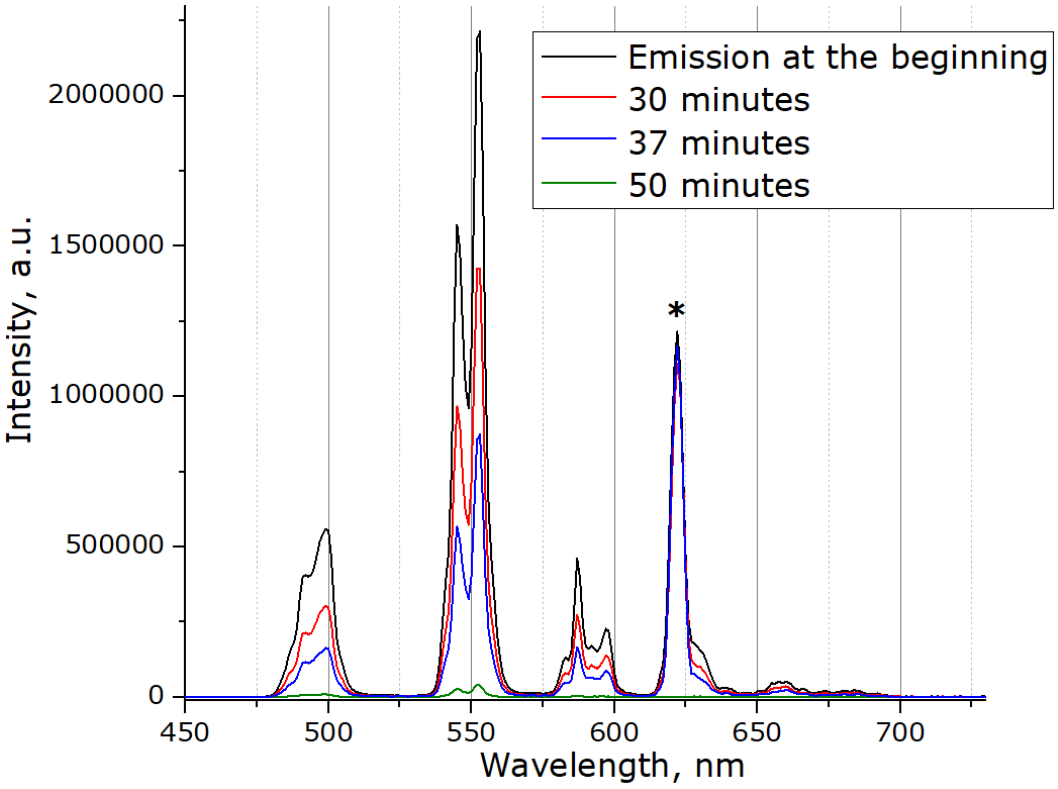

Figure S22 Decreasing emission of the solid sample **Tb^{Dipp}** during aging (λ_{em} = 310 nm). The band marked with * corresponds to the second-order diffraction artifact.

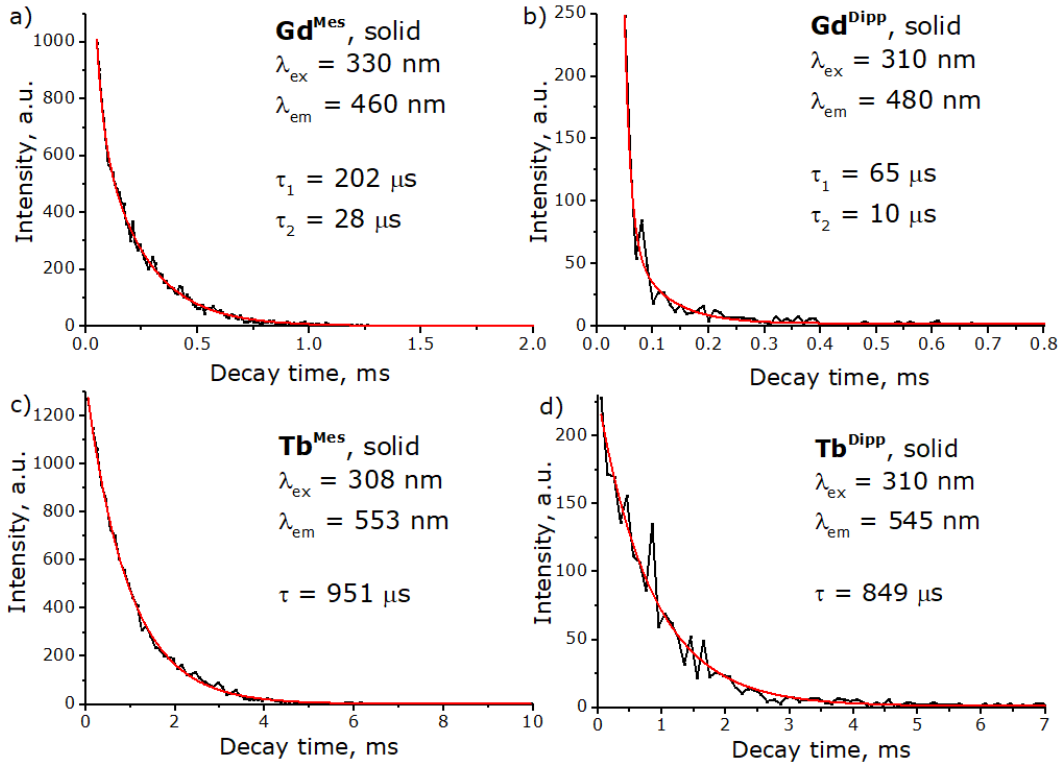

Figure S23 Emission decay curves of solid samples of **Ln^{Dipp}** and **Ln^{Mes}** (Ln = Gd, Tb).

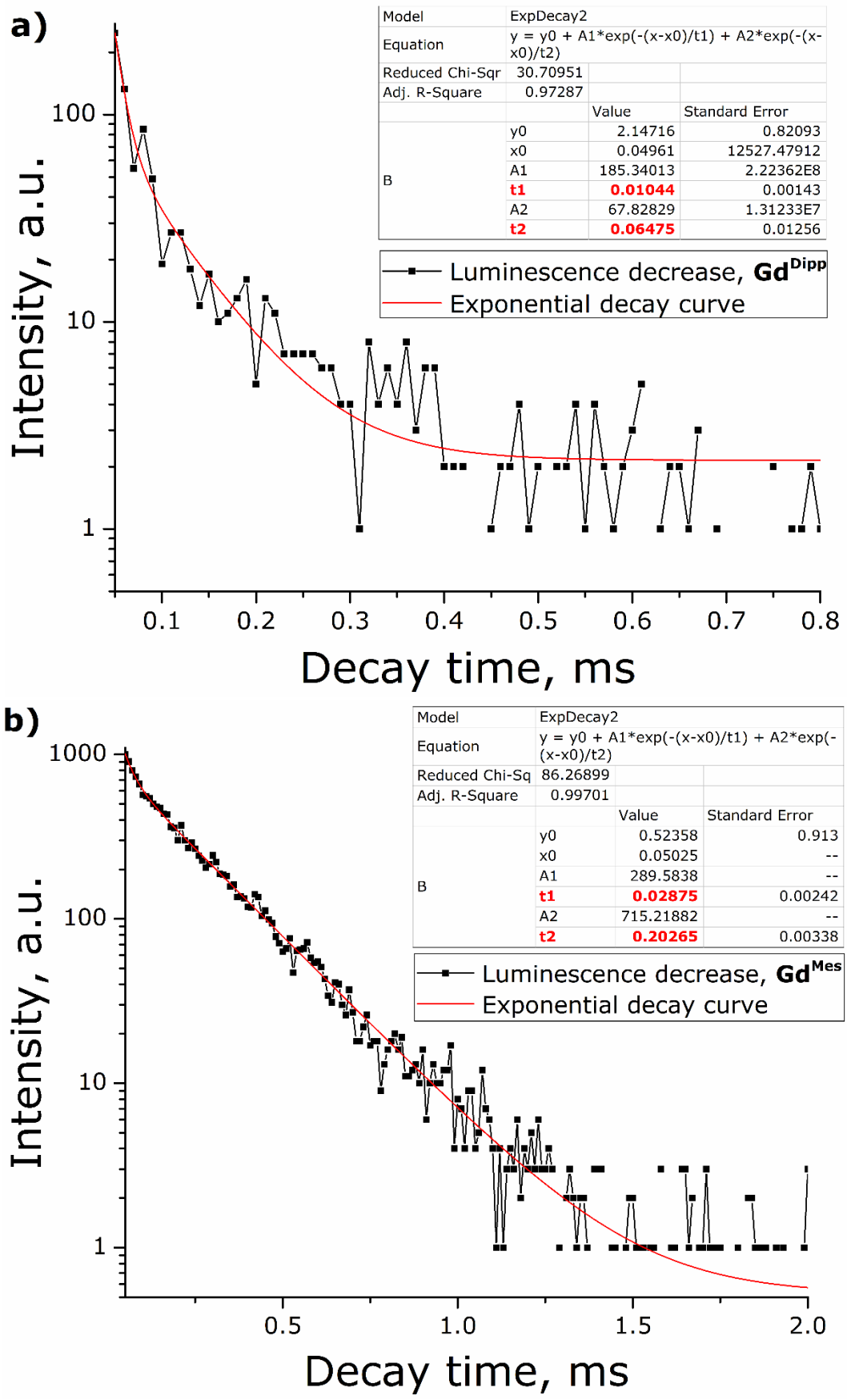

Figure S24 Emission decay curves of solid samples of a) $\mathbf{Gd^{Dipp}}$ and b) $\mathbf{Gd^{Mes}}$ (logarithmic scale).

6. Photos of the samples

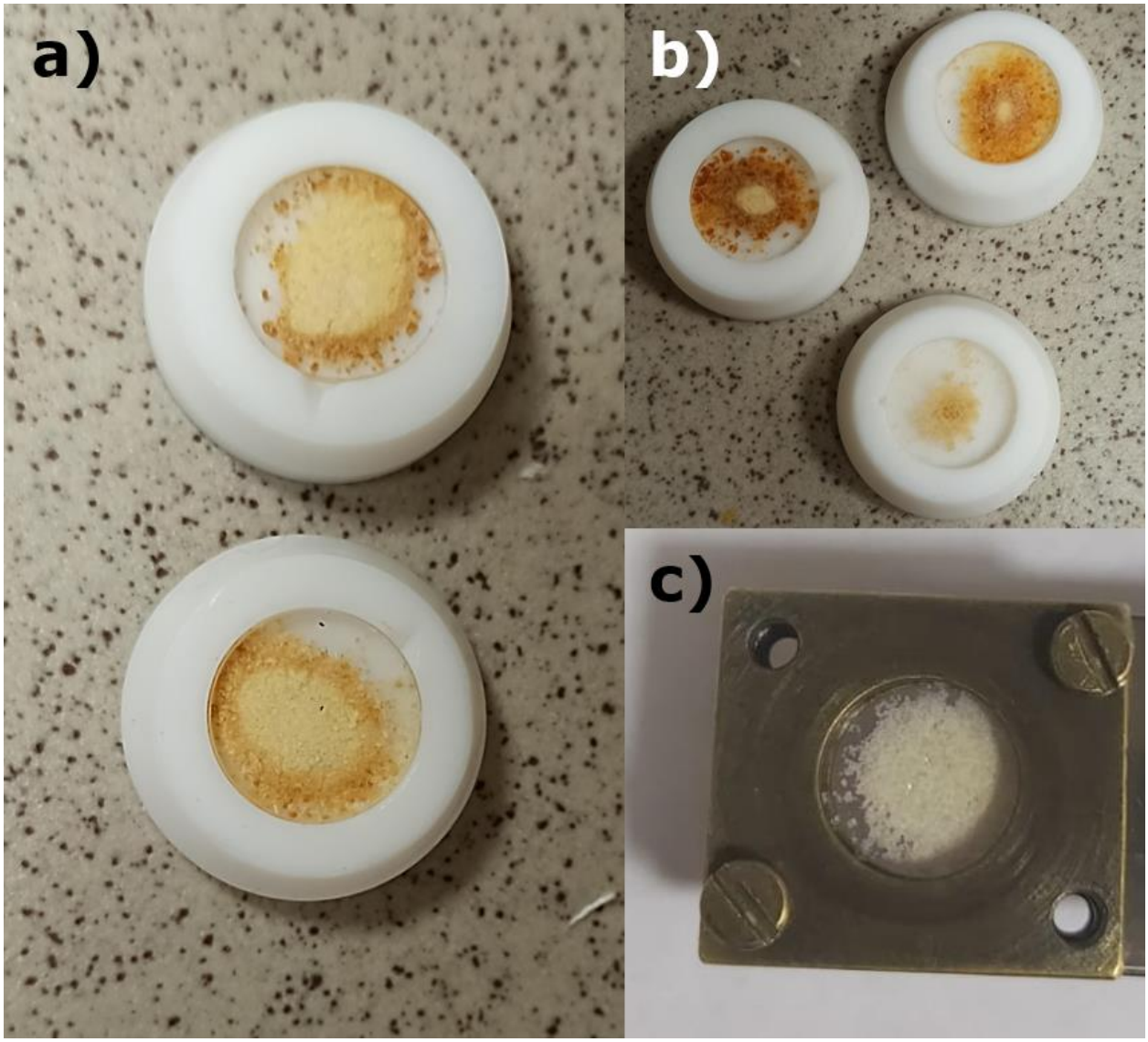

Figure S25 Photos showing degradation of samples of the complexes for the luminescent studies in air visually observed as darkening of the sample edges. a) samples in Teflon cuvettes covered with glass after 15 min, b) after 30 minutes; c) no degradation of the sample placed in a two-wall glass cuvette for low-temperature measurements.